ULTRAVIOLET TRANSVERSE SHAPING WITH STRUCTURED-STOCHASTIC PHASE-PLATES FOR PHOTOCATHODE APPLICATIONS*

T. Jogand-Coulomb† [1], R. Margraf-O'Neal[2], N. Burdet[4], D. Czaplezski[2], R. Divan[2], J. Xu[3], A. Osman[4], J. Power[2], A. Halavanau[4], P. Piot[2], Y.K. Kim[1,5]
[1]University of Chicago, Chicago, USA
[2]Argonne National Laboratory, Lemont, USA
[3]University of Wisconsin-Madison, Madison, USA
[4]SLAC National Accelerator Laboratory, Menlo Park, USA
[5]Fermi National Accelerator Laboratory, Batavia, USA

Abstract

Transverse shaping of the photocathode drive laser can improve beam quality in high-brightness photoinjectors. We present progress on UV-compatible fused-silica phase plates for passive laser shaping at the Argonne Wakefield Accelerator. A first-generation binary phase plate, designed using an iterative Fourier transform algorithm, was fabricated and optically characterized. The measured Fourier-plane profile demonstrates transverse redistribution of the incident UV beam, while residual central intensity indicates sensitivity to binary phase quantization and etch-depth error. To address these limitations, we introduce an improved genetic algorithm workflow in which structured initial phase seeds are optimized with an NSGA-II assisted IFTA. The resulting simulated four-level phase plates are selected using target-profile fidelity and zeroth-order diffraction intensity, providing a fabrication-aware path for next-generation devices.

INTRODUCTION

The performance and cost of electron accelerators depend critically on the transverse emittance of the electron beam [1–6]. This emittance depends partially on the initial conditions set by the photoinjector. There are three major areas of improvement for photoinjectors: (i) refining the transverse profile, (ii) reducing transverse jitter, (iii) reducing charge jitter. Addressing these challenges would reduce tune-up time and allow for more stable beam delivery and experimental uptime.

Despite advances in existing shaping techniques such as spatial light modulators [7, 8] and digital mirror devices [9], these techniques still incur significant power losses or lack compatibility with UV drive wavelengths. To overcome these limitations, recent work [10] has demonstrated that custom fused-silica phase plates, designed using an optical Iterative Fourier Transform (IFTA) [11], can generate high-precision transverse UV profiles while maintaining greater than 99% transmission at 253 nm. These phase plates provide a passive solution for tailoring laser distributions without sacrificing energy at the cathode. This project aims to adapt and extend phase-plate technology specifically for the Argonne Wakefield Accelerator (AWA) photoinjector.

BINARY PHASE PLATE

A binary phase plate was designed to transversely shape an incident UV beam into a truncated, flat-top transverse profile at the Fourier plane. This 2-level phase mask, with discrete phase levels of 0 and π, was designed using an Optical-IFTA workflow (Fig. 1) from previous work [10]. This phase plate serves as a proof-of-principle that the simulation could be applied to fabricate a phase plate for AWA while also identifying the limitations that motivate the optimized multi-objective designs discussed in the following section.

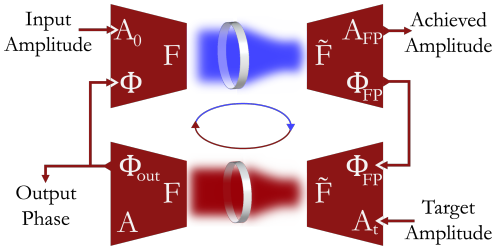

Figure 1: Schematics of the Optical IFTA implemented to generate the phase masks.

The binary plate was fabricated at the Center for Nanoscale Materials on a UV fused-silica substrate using a single lithography and etch step. The etched depth d sets the phase delay according to

$$\Delta\phi = \frac{2\pi}{\lambda}\left(n_{\mathrm{fs}} - n_{\mathrm{air}}\right) d, \tag{1}$$

where λ is the operating wavelength and n_{fs} and n_{air} are the refractive indices of fused silica and air. Optical microscopy was used to verify the transverse pattern fidelity, while atomic force microscopy (AFM) measured the etched step height, as shown in Figs. 2 and 3. From this metrology, the transverse feature size area agreed with the design, with $A_{\mathrm{etch}} = 38 \pm 2\ \mu\mathrm{m}^2$ compared with $A_{\mathrm{design}} = 38.4\ \mu\mathrm{m}^2$. However, AFM showed a significant etch-depth error of $\delta h = 78.0 \pm 0.1$ nm relative to the target π-phase depth. This depth error changes the intended phase step and contributed residual zeroth-order diffraction in the Fourier plane.

* Work supported by DOE Award DE-SC0024907
† coulomb@uchicago.edu

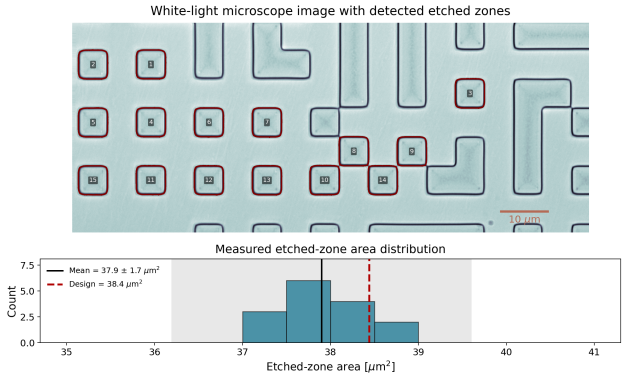

Figure 2: White light microscope image of a section of the binary phase plate with an analysis of the area of each etched pixel from simulation.

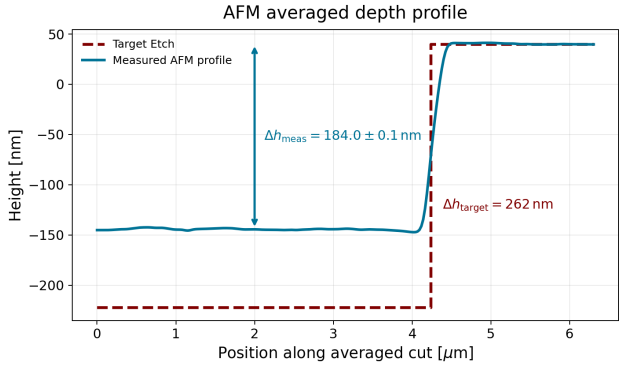

Figure 3: Averaged AFM lineout of the etched binary phase step compared with the target π-phase depth.

Phase plate validation was carried out at AWA's photoinjector. The UV drive laser was expanded and collimated with a two-lens telescope, transmitted through the phase plate and imaged at the Fourier plane on a YAG screen. The screen emission was recorded with a camera and compared with the simulated Fourier-plane intensity. Figure 4 shows that the fabricated plate transversely shapes the incident UV beam in qualitative agreement with the simulation. The measured profile exhibits strong central intensity, consistent with residual zeroth-order diffraction from etch-depth error and binary phase quantization. This result validates the fabrication and beamline workflow, but shows that future masks must be optimized using metrics beyond target-profile error alone.

GENETIC ALGORITHM OPTIMIZATION

The first-generation binary phase plate demonstrated passive UV transverse shaping with a nanofabricated fused-silica optic, but also showed that minimizing target-profile error alone is insufficient. The measured beam quality depended greatly on residual zeroth-order light and sensitivity to etch-depth errors. These limitations motivated a GA-assisted extension of the IFTA workflow, where structured initial phase seeds for the IFTA are optimized rather than manually selected.

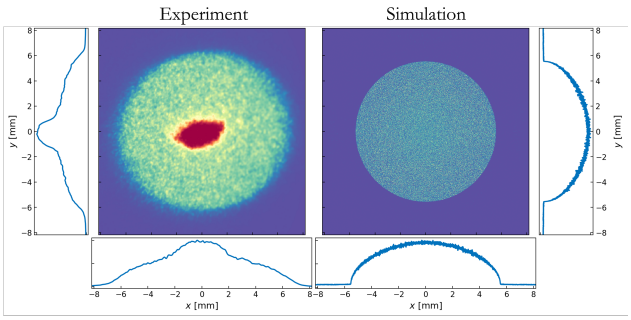

Figure 4: Comparison of measured and simulated Fourier-plane intensity for the first-generation binary phase plate tested at AWA.

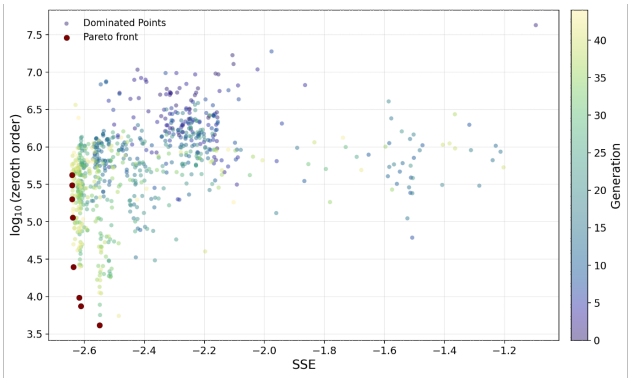

Figure 5: Distribution of candidates for the multiobjective optimization over SSE and zeroth order intensity.

The initial phase seed combines spiral-zone-plate (SZP) modes [12] with a small basis of high-performing random phase arrays,

$$\phi_{\text{seed}} = \sum_i \alpha_i \Psi_i + \sum_j \beta_j \Phi_j(f_j), \tag{2}$$

where Ψ_i are fixed random phase arrays, Φ_j are SZP phases of order j, α_i and β_j set their weights and f_j sets the SZP focal length of each SZP_j. The resulting phase is then wrapped modulo 2π and used as the initial condition for the IFTA.

The structured seed parameters are then optimized using the NSGA-II [13] through Xopt [14]. Each individual in the population corresponds to a vector of seed parameters,

$$\mathbf{p} = (\alpha, \beta, \mathbf{f}), \tag{3}$$

which defines an initial phase seed through Eq. (2). For each individual, the seed is passed to the IFTA routine, producing a candidate phase plate. The candidate is then scored through several objective metrics. The primary objectives to minimize are the normalized Sum Squared Error (SSE) [15] which measures the overall agreement with the desired profile and the zeroth-order diffraction intensity from Eq.5. Candidates are ranked by NSGA-II selection, then recombined and mutated to form the next generation. After hypervolume convergence [16], representative masks are chosen from the Pareto front for further analysis as shown in Figure 5.

The GA workflow was used to generate simulated four-level phase-plate candidates where the phase is quantized

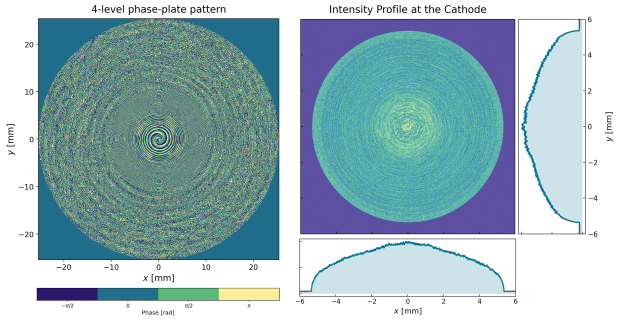

Figure 6: Simulated output of a Pareto front candidate of a 4-level phase plate.

such that,

$$\Phi(x,y) \in \left\{0, \frac{\pi}{2}, \pi, \frac{3\pi}{2}\right\}. \tag{4}$$

The additional phase levels reduce quantization error and are expected to suppress zeroth order contribution relative to a binary mask. These four-level designs (Fig. 6) have not yet been fabricated, but they define the target architecture for the next iteration of fabrication.

FABRICATION TOLERANCE

For a phase mask $\Phi(x,y)$, the zeroth-order amplitude is found by integrating over the phase mask [17],

$$A_0 = \frac{1}{A}\int_A e^{i\Phi(x,y)}\, dA. \tag{5}$$

Then, for a 4-level phase plate where we etch 2 separate substrates such that,

$$\Phi = \Phi_1 + \Phi_2, \quad \Phi_1 \in \{0, \pi\}, \quad \Phi_2 \in \left\{0, \frac{\pi}{2}\right\}. \tag{6}$$

From here, we can define,

$$\alpha = \pi + \Delta\phi_1, \quad \beta = \frac{\pi}{2} + \Delta\phi_2, \tag{7}$$

where $\Delta\phi_1$ is the error on the π etch and $\Delta\phi_2$ is the error on the $\pi/2$ etch such that, when assuming equal amounts of each phase in the 4-level mask, we obtain,

$$A_0 = \frac{1}{4}(1 + e^{i\alpha})(1 + e^{i\beta}). \tag{8}$$

$$\therefore I_0 = \sin^2\left(\frac{\Delta\phi_1}{2}\right)\cos^2\left(\frac{\pi}{4} + \frac{\Delta\phi_2}{2}\right), \tag{9}$$

where at first order, the zeroth order intensity is proportional to quadratic etch errors in $\Delta\phi_1$ but only linear in $\Delta\phi_2$. This implies the error on the $\pi/2$ etch is negligible compared to the error on the π etch for small etching errors; which was confirmed by our simulations shown in Figure 7, where the tolerance in etch was improved to a 4 nm band compared to the 2 nm band we find for a binary phase plate.

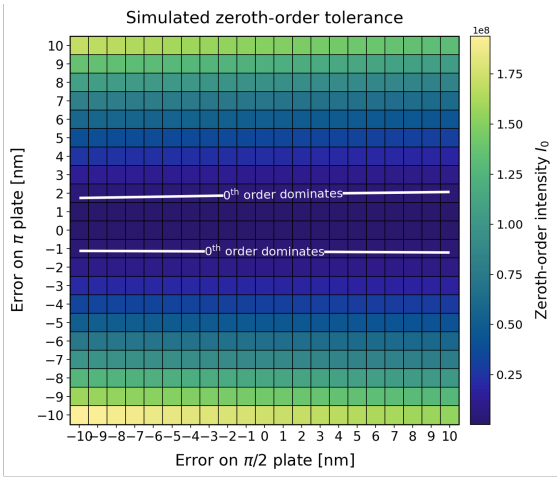

Figure 7: Simulated zeroth-order intensity as a function of etch-depth error for a four-level phase plate. The area within the lines is where the zeroth order does not dominate the profile.

CONCLUSION

A first-generation binary fused-silica phase plate was fabricated and tested at the AWA photoinjector, demonstrating passive transverse shaping of a UV drive laser. The measured Fourier-plane profile showed qualitative agreement with simulation, while the residual central intensity identified binary phase quantization and etch-depth error as key limitations.

To address these limitations, we developed a GA-assisted IFTA workflow in which structured initial phase seeds are optimized with NSGA-II. The resulting designs are selected using both target-profile fidelity and zeroth-order diffraction intensity. We also analyzed the zeroth-order sensitivity of a two-substrate four-level architecture to etch-depth errors, showing that fabrication tolerances directly determine the intensity of the central hot-spot. Simulated four-level phase plates generated with this workflow reduce phase quantization error and improve zeroth-order suppression, providing the design basis and tolerance targets for the next fabrication iteration.

ACKNOWLEDGEMENTS

Work performed at the Center for Nanoscale Materials, a U.S. Department of Energy Office of Science User Facility, was supported by the U.S. DOE, Office of Basic Energy Sciences, under Contract No. DE-AC02-06CH11357.

REFERENCES

[1] A. Halavanau *et al.*, "Spatial control of photoemitted electron beams using a microlens-array transverse-shaping technique", *Phys. Rev. Accel. Beams*, vol. 20, no. 10, p. 103404, 2017. doi:10.1103/PhysRevAccelBeams.20.103404

[2] B. E. Carlsten, "New photoelectric injector design for the Los Alamos National Laboratory XUV FEL accelerator", *Nucl. Instrum. Methods Phys. Res., Sect. A*, vol. 285, no. 1-2, pp. 313–319, 1989. doi:10.1016/0168-9002(89)90472-5

[3] P. Emma *et al.*, "First lasing and operation of an ångstrom-wavelength free-electron laser", *Nat. Photon.*, vol. 4, no. 9, pp. 641–647, 2010. doi:10.1038/nphoton.2010.176

[4] K.-J. Kim, Z. Huang, and R. Lindberg, *Synchrotron radiation and free-electron lasers*. Cambridge, UK: Cambridge University Press, 2017. doi:10.1017/9781316677377

[5] S. Bettoni *et al.*, "Overview of swissfel dual-photocathode laser capabilities and perspectives for exotic fel modes", *High Power Laser Sci. Eng.*, vol. 9, e51, 2021. doi:10.1017/hpl.2021.36

[6] D. H. Dowell, "High brightness electron injectors for 4th generation light sources, lecture 1: introduction and motivation", USPAS Lecture Notes, SLAC, Menlo Park, CA, USA, 2010, https://uspas.fnal.gov/materials/10MIT/Lecture1_Intro_and_Motivation_text.pdf,

[7] C. Xu *et al.*, "Machine learning based spatial light modulator control for the photoinjector laser at FLUTE", in *Proc. IPAC'21*, Campinas, Brazil, May 2021, pp. 3332–3335. doi:10.18429/JACoW-IPAC2021-WEPAB289

[8] C. Koschitzki *et al.*, "Chirped pulse laser shaping for high brightness photoinjectors", in *Proc. FEL2022*, Trieste, Italy, Aug. 2022, pp. 22–26. doi:10.18429/JACoW-FEL2022-WEA04

[9] S. Li *et al.*, "Ultraviolet laser transverse profile shaping for improving x-ray free electron laser performance", *Phys. Rev. Accel. Beams*, vol. 20, no. 8, p. 080704, 2017. doi:10.1103/PhysRevAccelBeams.20.080704

[10] T. J.-C. et al., "Ultra-violet laser transverse shaping with phase plates", in *Proc. NAPAC2025*, Sacramento, CA, USA, pp. 876–879, Aug. 2025. doi:10.18429/JACoW-NAPAC2025-WEP092

[11] J. R. Fienup, "Reconstruction of an object from the modulus of its fourier transform", *Opt. Lett.*, vol. 3, no. 1, pp. 27–29, 1978. doi:10.1364/OL.3.000027

[12] A. Sakdinawat and Y. Liu, "Soft-x-ray microscopy using spiral zone plates", *Opt. Lett.*, vol. 32, no. 18, pp. 2635–2637, Sep. 2007. doi:10.1364/OL.32.002635

[13] K. Deb, A. Pratap, S. Agarwal, and T. Meyarivan, "A fast and elitist multiobjective genetic algorithm: nsga-ii", *IEEE transactions on evolutionary computation*, vol. 6, no. 2, pp. 182–197, 2002.

[14] R. Roussel, A. Edelen, A. Bartnik, and C. Mayes, "Xopt: a simplified framework for optimization of accelerator problems using advanced algorithms", in *Proc. IPAC'23*, Venezia, pp. 4796–4799, May 2023. doi:doi:10.18429/jacow-ipac2023-thpl164

[15] C. Guo, S. Liu, and J. T. Sheridan, "Iterative phase retrieval algorithms. i: optimization", *Appl. Opt.*, vol. 54, no. 15, pp. 4698–4708, 2015. doi:10.1364/AO.54.004698

[16] A. P. Guerreiro, C. M. Fonseca, and L. Paquete, "The hypervolume indicator: computational problems and algorithms", *ACM Computing Surveys (CSUR)*, vol. 54, no. 6, pp. 1–42, 2021. doi:10.1145/3453474

[17] J. W. Goodman and M. E. Cox, "Introduction to fourier optics", 1969, doi:10.1063/1.3035549,